8-2019

# Change in the Leading Mode of North America's Wintertime Stationary Eddies

Yu-Tang Chien
*Utah State University*

CHANGE IN THE LEADING MODE OF NORTH AMERICA'S WINTERTIME STATIONARY EDDIES

by

Yu-Tang Chien

A thesis submitted in partial fulfillment
of the requirements for the degree

of

MASTER OF SCIENCE

in

Climate Science

Approved:

| | |
|---|---|
| Simon Wang, Ph.D.<br>Major Professor | Jonathan Meyer, Ph.D.<br>Committee Member |
| Steve L. Voelker, Ph.D.<br>Committee Member | Richard S. Inouye, Ph.D.<br>Vice Provost for Graduate Studies |

UTAH STATE UNIVERSITY
Logan, Utah

2019

# ABSTRACT

Change in The Leading Mode of North America's Wintertime Stationary Eddies

by

Yu-Tang Chien, Master of Science

Utah State University, 2019

Major Professor: Simon Wang, Ph.D.
Department: Plants, Soils and Climate

In recent years, extreme winter weather events in North America have become more frequent and increasingly destructive. The 2012-2015 wintertime California drought has been linked to the abnormal atmospheric high-pressure ridge, while the eastern U.S. undergo the cold anomaly event, forming an atmospheric pattern referred to as the North America winter Dipole. Several studies have demonstrated that the Dipole may have amplified and this amplification could be linked to anthropogenic warming. In this study, we utilized multiple global reanalysis datasets and empirical orthogonal function (EOF) analysis to (1) explore whether the long-wave pattern in the Northern Hemisphere during wintertime has changed and (2) better understand about the Dipole pattern in the present, past and future by analyzing the Dipole structure. In the first portion of this study, we compared between pre- and post- 1980 periods to identify the change of the circulation based on the EOF analysis and examined the air-sea interaction by the correlation analysis between the Principle component (PC) and the sea surface temperature. It was found that the leading EOF pattern of the winter circulation over North America has changed since the late 1980's, from the Pacific-North America (PNA) mode to the Dipole mode. Neither mode is a new climate pattern, but their "switch" in the variance explained has not been documented. In the second portion of this study, we tested multiple global reanalysis datasets to derive

the Dipole index and showed that the Dipole variance has undergone a pronounced low-frequency fluctuation. We further used all available teleconnection indices to identify their changing association with the Dipole pattern. Moreover, we investigated the Dipole index behavior under the paleoclimate and the double $CO_2$ future scenario.

(39 pages)

# PUBLIC ABSTRACT

Change in The Leading Mode of North America's Wintertime Stationary Eddies

Yu-Tang Chien

Extreme winter weather events in North America have become more frequent and increasingly destructive. This phenomenon was linked to a jet stream pattern that generates abnormally warm conditions in the west and cold conditions in the east, referred to as the North American Winter Dipole. Studies have shown that the Dipole may have amplified and this amplification could be linked to global warming. By analyzing the atmospheric and oceanic data worldwide, the wintertime circulation in the Northern Hemisphere shows signs of a persistent change after the 1980s. In the first part of this study, we examine how the ocean has changed in correspondence to the Dipole and the evolution of the pattern change. In the second part of this study, we use multiple global reanalysis datasets to construct the Dipole index. The result validates the reported Dipole variation during the modern period. We also use the Dipole variance to investigate the Dipole's behavior in the paleoclimate and future warming conditions. Overall, we sought to better understand how the Dipole pattern evolves and how it may link to the different forcing, as a way to anticipate future change in North America's winter.

# ACKNOWLEDGMENTS

I would first like to thank my thesis advisor Simon Wang for his support, guidance, and answers to my endless questions throughout this process. I would also like to thank my committee members, Dr. Jonathan Meyer, and Prof. Steve Voelker, for providing their expertise to this study and for always having helpful advice when it was needed. I also appreciate Prof. Yoshimitsu Chikamoto for additional suggestions for improving this study. Thank Yen-Hen (Henry) Lin for his tireless assistance in programming, and Boniface Fosu for his encouragement when I was under depression. Finally, I would like to thank Mr. Don. J. Wang for making my study at Utah State University possible.

Yu-Tang Chien

CONTENTS

# LIST OF FIGURES

# ACRONYMS

| | |
|---|---|
| 20CR | NOAA Twentieth Century Reanalysis version 2c |
| AO | Arctic Oscillation |
| AGCM | Atmospheric General circulation model |
| B.P. | Before Present, 1950A.D. |
| CESM | Community Earth System Model |
| ECMWF | European Centre for Medium-Range Weather Forecasts |
| ERA-20C | ECMWF global reanalysis products for the twentieth century |
| EOF | Empirical Orthogonal Function |
| ENSO | El Nino/ Southern Oscillation |
| LGM | Last Glacial Maximum |
| NH | North Hemisphere |
| NOI | Northern Oscillation index |
| PC | Principle Component |
| PDO | Pacific Decadal Oscillation |
| PNA | Pacific-North America |
| SST | Sea surface temperature |
| SSTA | Sea surface temperature anomaly |
| TNH | tropical Northern Hemisphere pattern |
| WAF | Wave activity flux |
| WNP | Western North Pacific pattern |
| WP | Western Pacific pattern |

# CHAPTER 1

# INTRODUCTION

According to the National Centers for Environmental Information report (NOAA 2019), during 1985-2005, Florida was the only state suffering billion-dollar losses related to freeze events in the eastern U.S. After 2006, the number of eastern states affected by these costly freeze-related disasters has doubled, along with a marked increase in the number of billion-dollar disasters caused by drought in western states. In the winter of 2013-2014, the exceptionally dry conditions in the West coast were accompanied by a persistent geopotential ridge located in the North Pacific. This ridge pushed storm tracks further north, resulting in wetter than normal conditions over the northwest of the United States and substantial drying over the southwest. Some studies showed that the striking division of the drought in the west and cold-snaps in the east have resulted from an atmospheric pattern referred to as the "North American Winter Temperature Dipole" (Singh et. al. 2016) or the "North American Winter Dipole" (Wang et. al. 2015), hereafter Dipole.

The polarity and location of this Dipole coincide with the wintertime stationary waves over North America, which feature a high-pressure ridge in the west and a low-pressure trough in the east. Oscillating in sync with the stationary waves, the positive-phase Dipole is associated with an anomalous ridge over the Gulf of Alaska and a deepened trough near the Great Lakes, thereby enhancing the east-west temperature contrast in North America (Voelker et al. 2019). Past studies suggested that the ridge in western U.S. (Swain et al. 2014) and the Dipole itself have amplified (Singh et. al. 2016), owing to internal and external variabilities, such as tropical Pacific heating (Hartmann 2015; Schulte and Lee 2017) and Arctic warming (Francis and Varus 2012; Overland et al. 2016). The intense Dipole reversal seen in the winter of 2016-17 suggests that the variation amplitude also increases, accompanying the wet winter in California (Wang et al. 2017; Swain et al. 2018). These observations imply a change in the atmospheric circulation regime over North

America, which is examined herein.

This study explores the wintertime leading pattern evolution in North America and diagnoses forcing sources. While the 2013/2014 extreme event has been extensively studied, the role of large-scale climate variability has not been satisfactorily addressed. Understanding the major wintertime circulation pattern evolution over Northern America, as well as the dipole index variance from the paleoclimate to the future projection, can allow us to better predict future. In the first portion of this study (Chapter 2), the overarching goal was to examine the dominant patterns during the recent decades and to compare with the known climate pattern: Pacific-North American (PNA) and Dipole pattern. In this study, geopotential height at 250 hPa is the main component we analyzed. By removing the zonal average and focus only on the November to January monthly data, Empirical Orthogonal Function (EOF) analysis gave us the major circulation pattern of the North Hemisphere. Furthermore, spacial correlation analysis was applied to compare the EOF results and the other patterns in order to capture the leading pattern feature. In the second portion of this study (Chapter 3), we use multiple global reanalysis datasets to derive dipole index and its variance to verify whether the variation of the Dipole index is consistent during the analysis period. This portion of the study also explored the correlation between the teleconnection indices based on literature review as well as dipole variability under the paleoclimate data and the Community Earth System Model (CESM) simulation with Representative Concentration Pathways (RCP) 8.5 "high emission" future scenarios. Combined, we anticipate to investigate the potential forcing and whether the Dipole pattern will last. This analysis gives us a better point of view about the future of wintertime extreme events.

# CHAPTER 2

# CHANGE IN THE LEADING CIRCULATION PATTERNS

## 2.1 Introduction

This study explores the wintertime leading pattern evolution in North America through the perspective of the long-term time scale. The most well-studied teleconnection pattern which affects North America is arguably the Pacific-North American (PNA) pattern. The PNA is a low-frequency variability mode in the Northern Hemisphere, which influences regional weather by affecting the strength and location of the East Asian jet stream, and subsequently, the weather it channels to North America. The PNA involves changes in atmospheric pressure between the Aleutian Low and the high pressure over the Rocky Mountains. This situation increases the likelihood of above-average temperatures over western Canada and the western states of the U.S., and below-average temperatures across south-central and southeastern states. The PNA can impact crop production and the growing season. In winter, the positive-phase PNA is associated with below-average precipitation in the Pacific Northwest and across the eastern half of the United States. Although the PNA pattern is an internal mode of climate variability, it is also strongly influenced by the El Nino/ Southern Oscillation (ENSO) phenomenon. The positive phase of the PNA tends to be associated with ENSO warm episodes (El Nino), and the negative phase tends to be associated with ENSO cold episodes (La Nina).

The division of western U.S. drought and eastern U.S. cold-snaps have resulted from an atmospheric pattern referred to as the "North American Winter Temperature Dipole" mainly from the perspective of the surface temperature (Singh et. al. 2016) and the "North American Winter Dipole" from the perspective of the 250 hPa geopotential height (Wang et. al. 2015). Interestingly, the intense Dipole reversal seen in 2016-17 winter suggests that the variation amplitude also increases, leading to extreme conditions such as wet winters

in California (Wang et al. 2017; Swain et al. 2018). Therefore, we examine the change in climate circulation characteristics and their role in the North America winter through the angle of variation in the North America circulation.

## 2.2 Data and methods

### 2.2.1 Reanalysis data

The primary dataset used to study the atmospheric circulation features of interest is the NCEP–NCAR re-analysis (Kalnay et al. 1996) from 1948-present. The re-analysis project provided global gridded fields produced with a comprehensive objective analysis system with a large input database (including data available after the operational cutoff time). Although the satellite data was lacking before 1979, the temporal coverage of this re-analysis is longer than newer re-analysis that inquests satellite data. Thus, when interpreting the early 20th-century climate, we need to be cautious to avoid over-interpretation. We also used the National Oceanic and Atmospheric Administration (NOAA) Extended Reconstructed Sea Surface Temperature (ERSST) V4 dataset, starting in 1854 with a 2° spatial resolution (Huang et al. 2014), and the European Centre for Medium-Range Weather Forecasts (ECMWF) interim reanalysis (ERA-Interim; Dee et al., 2011) from 1979 to 2015 and extend back to 1958 by concatenating with ERA-40 (Uppala et al., 2005). Additionally, we used a retrospective reanalysis dataset to depict the global atmospheric circulation: the ECMWF global reanalysis products for the twentieth century (ERA-20C) (Poli et al. 2016) from 1871–2012. Based on large ensembles, 20CR (ERA-20C) utilized a coupled Atmosphere/Land-surface/Ocean model to assimilate surface observations of sea level pressure (surface pressure) to produce the atmospheric conditions. It should be noticed that the 20CR dataset is developed from the model simulation forced by surface conditions only, therefore, it is not a full re-analysis. In this study, we mainly utilized by the monthly mean North Hemisphere geopotential height from November to February that are available on a 2.5 times 2.5 long grid.

### 2.2.2 EOF Analysis

The Empirical orthogonal function (EOF) and Principal Component analysis (PCA) are the main analysis technique for this study. According to Jolliffe (2002, p 1), the central idea of EOF/PCA is to reduce the dimensionality of a data set consisting of a large number of interrelated variables while retaining as much as possible of the variation present in the data set. This is achieved by transforming to a new set of variables, the principal components, which are uncorrelated, and which are ordered so that the first few retain most of the variation present in all of the original variables. In its simplest formulation, EOFs are eigenvectors of the data covariance matrix. The eigenvectors are commonly referred to as modes. Suppose the data are arranged in a matrix with 'time' being column dimension and 'space' being the row dimension. Then covariance can be computed over time as is typically done for time series data. It can be shown that the eigenvectors of the covariance matrix are related to the eigenvalues of the data matrix.

Because of this technique is a decomposition of a signal or data set in terms of orthogonal basis functions and seeks spatiotemporally-coordinated structures that explain maximum variance, which is determined from the data construction, this study was subjected the monthly anomalies of geopotential height (Z) at 250 hPa from November through February, with the zonal mean removed to depict the stationary eddies (herein $\triangle Z_E 250$). Considering the grid data in the high latitude has higher resolution, we emphasize the signal in tropical region by the cosine weight as a function of latitude. By doing so, we can balance the signal from the tropical and from the polar region. The month-by-month arrangement of $\triangle Z_E 250$ reflects the strong sub-seasonal variability of winter climate over North America (Higgins et al. 2000). The EOF/PC analysis provides simple representations of the spatial state of atmospheric circulations, which do not evolve with time. This restricts the EOF/PC technique for investigating trends presented as shifts of or changes in spatial pattern. Therefore, the running time window strategy from Zhang et al. (2008), called the Running-EOF analysis, was conducted. In this way, we use running 30-year period, each EOF analysis contains 120 realizations (30 years $\times$ 4 months).

### 2.2.3 Spatial correlation analysis

Spatial correlation falls into two types: auto-correlation and cross-correlation. The former reflects a relation between one measure and itself, while the latter reflects a relationship between one measure and another measure. To illustrate further the relationship between EOF results and the Pacific North America/Dipole pattern, a linear spatial cross-correlation function is adopted. The aim of this technique is simply to get the accuracy/similarity of spatial patterns between two variables over an X-Y domain.

### 2.2.4 Wave Activity Flux Analysis

The wave-activity flux is a useful diagnostic tool for illustrating a "snapshot" of a propagating packet of stationary or migratory Quasi-Geostrophic (QG) Rossby wave disturbances and thereby for inferring where the wave packet is emitted and absorbed. We use the source code derived by Takaya and Nakamura (2001, JAS: TN01) in GrADS.

## 2.3 Results

### 2.3.1 Evolution of the change

We use multiple global reanalysis data sets, including NCEP–NCAR reanalysis (Kalnay et al. 1996) from 1948-present, European Centre for Medium-Range Weather Forecasts (ECMWF) interim re-analysis (ERA-Interim; Dee et al., 2011) from 1979 to 2015 and extend back to 1958 by concatenating with ERA-40 (Uppala et al., 2005), and a retrospective reanalysis datasets to depict the global atmospheric circulation: the ECMWF global reanalysis products for the twentieth century (ERA-20C) (Poli et al. 2016) from 1871–2012. To examine the evolution in which the leading mode of $\triangle Z_E 250$ started to change, we adopted the running-EOF method (Zhang et al. 2008). A series of EOF analysis was conducted in the 30-year window and repeated every five years. The leading EOFs are then subject to a spatial correlation analysis with the PNA pattern and the Dipole pattern, which is delivered from the EOF 1 results of the 1950-1980 geopotential height based on the Climate Prediction Center, and from 2013/2014 wintertime circulation based on

the definition of Dipole by Wang, et al. (2015) respectively. Through this process, the results formed a series of correlation coefficients with each 30-year period. This analysis was performed on three reanalysis datasets: ECMWF 20-Century Reanalysis (ERA20C), the ERA-Interim, and NCEP-NCAR reanalysis I. As shown in Fig. 2.1, the running-EOF results illustrate a decreasing trend in the correlation between EOF1 and PNA from 1970 to 2000. Meanwhile, the correlation increases between EOF1 and the Dipole, computed from the $\triangle Z_E 250$ of the 2013-2014 winter (Wang et al. 2014). Correspondingly, sliding correlations of the second running-EOF (EOF2) with the PNA show an opposite trend (Fig. 2.1 b), suggesting that the Dipole used to be the second mode, but it has intensified while overtaking EOF1 during the 1990s.

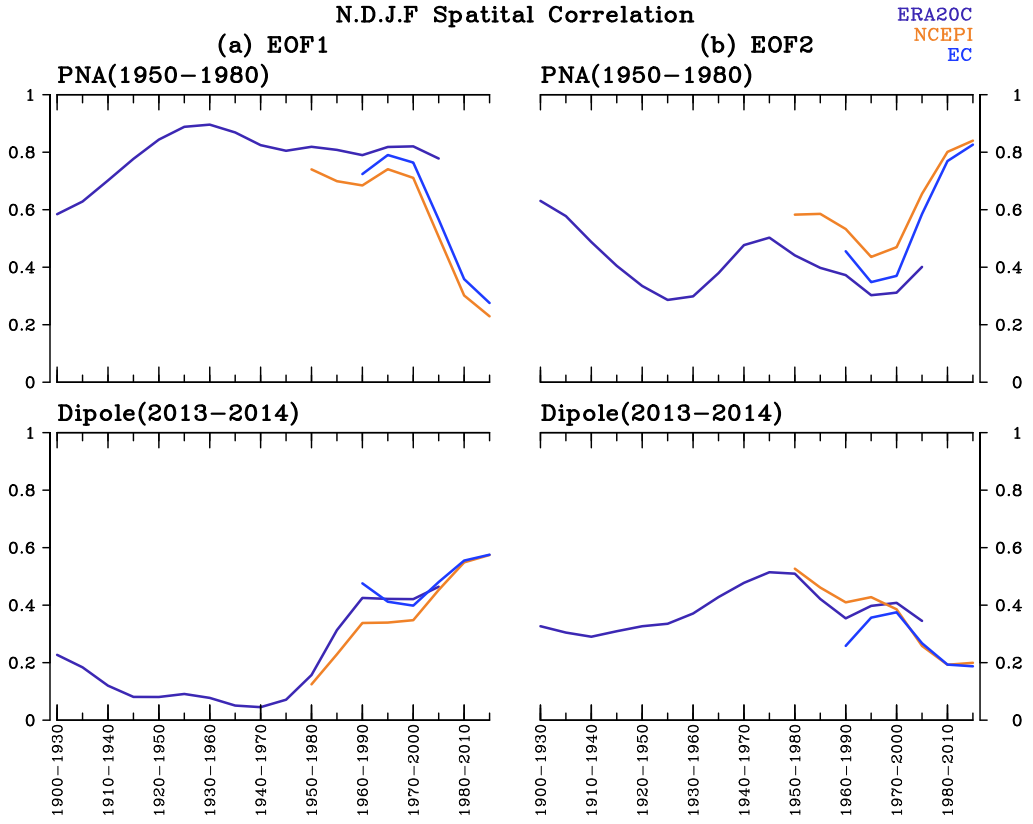


Fig. 2.1: Spatial correlation coefficients between the PNA/Dipole pattern and (a) EOF 1, during 1948-1979 (b) EOF 2, during 1980-2017 of $\triangle Z_E 250$. This analysis is repeated throughout a 30-year Running-EOF window done every 5 years using three different reanalysis data sets as indicated on top of (b).

The mechanism behind this decadal shift in the prevailing modes of variation is manifold. Previous studies proposed that the ENSO-forced PNA would move eastward in response to the spatial shift of the mean SST warming (Zhou et al. 2014). Interdecadal variability of the North Pacific sea level pressure can induce a shift in the PNA (Johnson and Feldstein 2010). Moreover, one could relate the Dipole to the maintenance of wintertime stationary waves (*e.g.*, Chang 2009). The western ridge of the North American stationary waves is primarily linked to the orographic forcing of the Tibetan Plateau on the jet stream, while the Rocky Mountains amplify the eastern/downwind trough. Diabatic heating from the Western Pacific and North Pacific further enhances and shapes this ridge-trough pattern. Therefore, the observed Dipole amplification could be related to the combination of such forces, *i.e.* jet stream-terrain interactions and diabatic heating.

### 2.3.2 Change in leading patterns

By setting 1980 as the dividing year to distinguish the circulation pattern change, the first EOF mode of $\triangle Z_E250$ during the earlier period of 1948-1979 is shown in Figure 2.2. Explaining 18.6% of the variance, this leading EOF features a wave train emanating from the central Pacific to the U.S., coincident with the Pacific-North American (PNA) pattern. By superimposing the PNA contours, which was produced by correlating $\triangle Z_E250$ with the PNA index from the NOAA Climate Prediction Center, the two patterns of EOF1 and PNA are in-phase. By comparison, the post-1980 EOF1 (Fig. 2.2b) shows a similar wave train but the wave centers are shifted from the PNA pattern by about a quarter phase. It appears that the post-1980 EOF1 becomes phase coincident with the Dipole centers (marked with $\times$ and $+$ in North America). This result suggests that the leading mode of $\triangle Z_E250$ variability has changed from a PNA-like pattern to one that resembles the Dipole. However, by repeating the EOF analysis with seasonal means instead of monthly intervals, the leading pattern of the latter period would still be PNA, whereas the Dipole remains secondary (Fig. 2.3 a, Fig. 2.3 b). These results imply that the observed reversal from PNA to Dipole is mainly related to the sub-seasonal variability, an emerging subject of intense research nowadays.

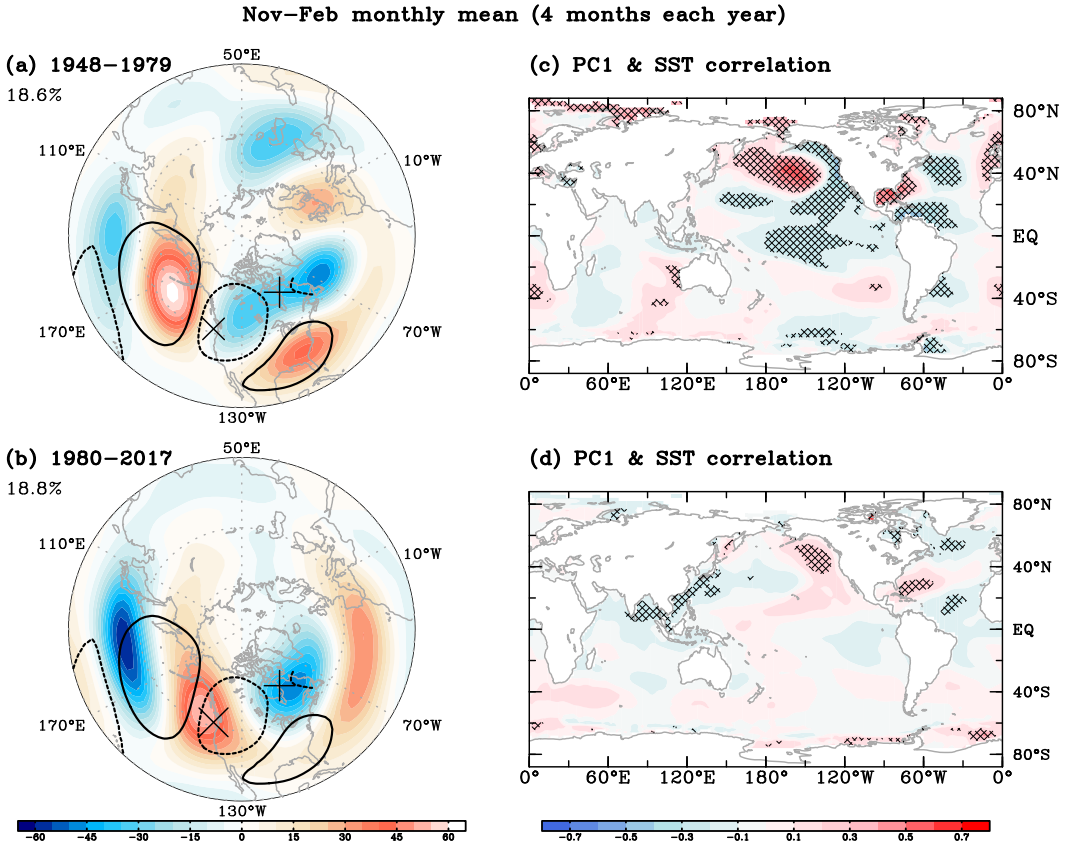


Fig. 2.2: First EOF mode of monthly $\triangle Z_E 250$ during (a)1948-1979 and (b) 1980-2017 winters (EOF1 shading), superimposed with the PNA pattern (contour) and the Dipole centers (marked with $\times$ and $+$) in North America. The correlation maps between monthly SST anomalies and the first principle component (PC1) are shown for the (c) 1948-1979 and (d) 1980-2017 periods. Hatched areas indicate significant values ($p < 0.01$). Percentage explains the variance of EOF result.

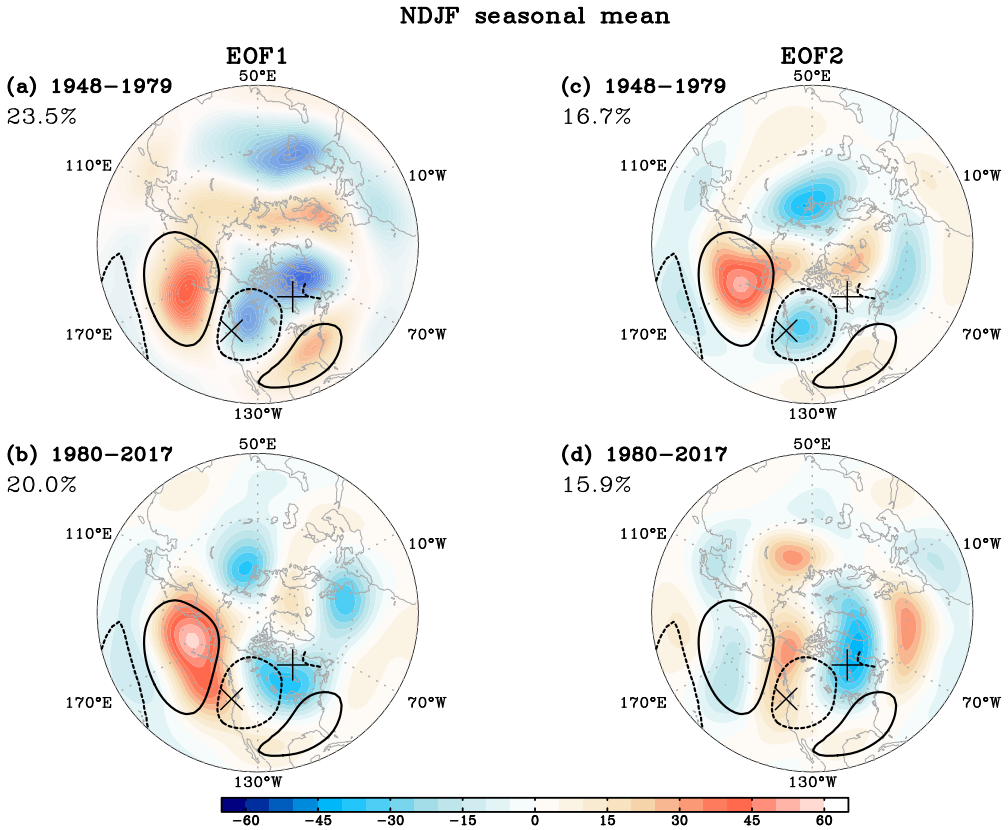


Fig. 2.3: First EOF mode of seasonal mean (NDJF) $\triangle Z_E 250$ during (a)1948-1979 and (b) 1980-2017 winters (shading) and Second EOF mode of seasonal mean (c) and (d). Superimposed with the PNA pattern (contour) and the Dipole centers (marked with $\times$ and $+$) in North America as in Fig. 2.2. Percentage explains the variance of EOF result.

To understand the air-sea interaction, we correlated the first principal component (PC1) time series with the monthly SST anomalies (Nov-Feb). The pre-1980 EOF1 corresponds to a La Niña-like pattern resembling the cold-phase Pacific Decadal Oscillation (PDO) (Fig. 2.2 c), which supports the associated PNA atmospheric wave train (Fig. 2.2 a). After 1980, the SST correlation map with respect to EOF1 changed dramatically and is absent of the PDO alongside most tropical signatures (Fig. 2.2 d). This post-1980 SST pattern corresponding to EOF1 reveals the oceanic "Blob" along the West coast (Kintisch 2015), as well as robust negative anomalies in the Western North Pacific and the Bay of Bengal. This latter SST feature coincides with an ENSO precursor, called the Western

North Pacific pattern (WNP), that saw amplification in recent decades (Wang et al. 2013). These results also echo the study by Kirtman et al. (2001), that sub-seasonal SST anomaly variability has a significant impact on North American climate anomalies. The marked difference between these SST patterns accompanying EOF1($\triangle Z_E 250$) of two eras implicates two very different modes of sub-seasonal variability influencing North American winter.

To clarify the change of the circulation, we conducted Wave Activity Flux (WAF) analysis (Takaya and Nakamura, 2001) on the U and V wind field at 250 hPa which has regressed with PC1 and PC2 from the previous results. A wave-like structure in the upper troposphere can be seen (Fig. 2.4). The horizontal wave activity flux has suggested two distinct forcing sources emanated from the tropics during the pre-1980 period and from the subtropics during the post-1980 period. Figure 2.4 illustrated that the wave train appears to originate from East Asia in the first period, conveys the energy from the tropics to the extratropics, which enhances the ridge over the Aleutian Islands. The response of the downstream wave separates into two directions, the major one toward the East coast of North America and the minor one through the southeast. The southeast US branch of wave activity flux appears to regenerate another wave train toward Europe. The post-1980 circulation has a different pattern, in which the forcing source shifted and expended to the north and Japan. The consequence of the source shifting is the change of the downstream wave activity flux. The ridge over the Aleutian region moved eastward to the Gulf of Alaska, and the wave train propagated northeastern North America. Notably, this wave train stays in North America without re-generating another trans-Atlantic wave train. This difference of the wave activity flux implies that, through the enhancement of the PNA wave train, ENSO can impact Europe, wheras the Dipole only affects North America.

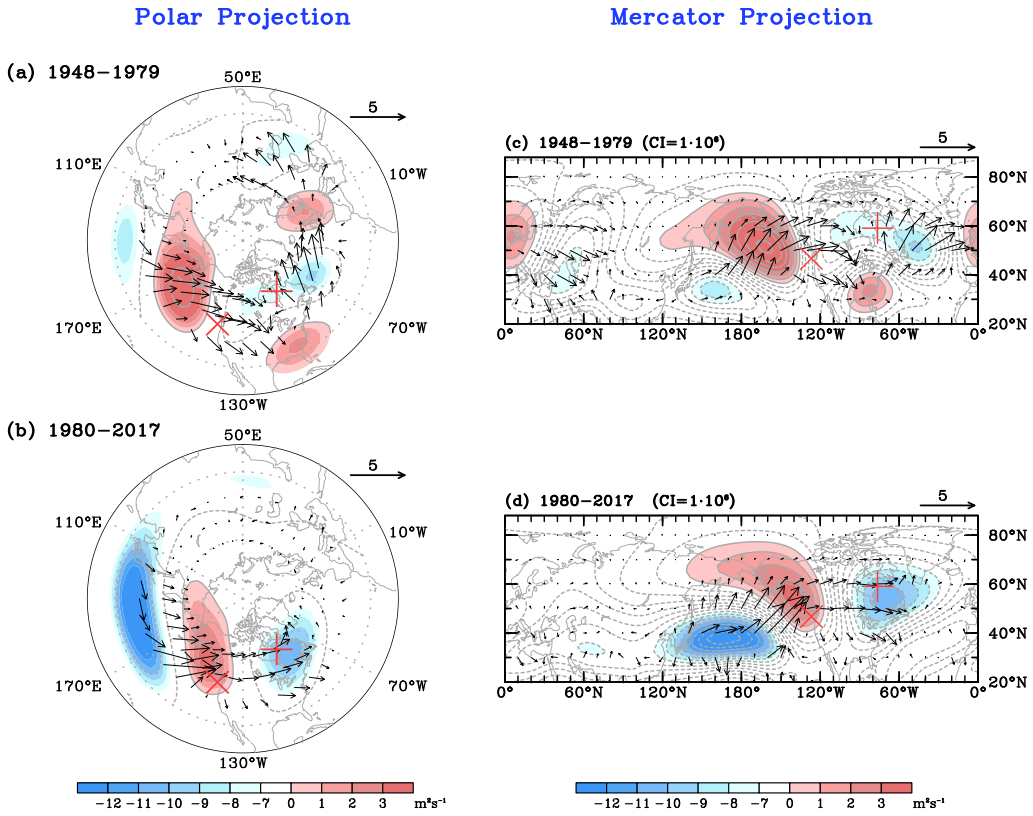


Fig. 2.4: The regressed NDJF monthly 250-hPa Streamfunction during (a)1948-1979 and (b) 1980-2017 for polar projection and (c) (d) for Mercator projection [gray contour; contour interval (CI) = $1*10^6$] associated horizontal component of the wave activity flux (arrow; unit: $m^2\ s^{-2}$).

## 2.4 Conclusion

In this study, we compared the wintertime leading circulation in North America during the pre- and post- 1980 by EOF analysis. We found that the pre-1980 dominant pattern is PNA-like while the post-1980 era resembles the Dipole pattern in terms of sub-seasonal variability. Further comparison of EOF1/EOF2 with PNA/Dipole pattern with spatial correlation reveals that the leading mode had changed over the analysis time. The PNA pattern changed from being the first leading mode to the second, while Dipole became from

the second mode to the first leading pattern. The mechanism of the pattern changing is unclear, which certain studies have argued about the feasible forcing source and/or theory (Johnson and Feldstein 2010; Chang 2009). The results portray a consistent pattern switching in three reanalysis datasets, suggesting that this change in the leading modes of wintertime North Hemisphere circulations is reliable. The underlying dynamics of the Dipole pattern enhancement is further examined with paleo and projection simulation in the next chapter.

# CHAPTER 3

# PRE-INDUSTRIAL AND FUTURE PERSPECTIVES

## 3.1 Introduction

In section 2, it was suggested that the North America wintertime circulation variability has evolved since the 1980s to one that is dominated by the Dipole pattern from that of the PNA pattern. This phenomenon was observed in three different datasets, revealing a decreasing PNA variance accompanied by an increasing Dipole variance during recent decades. Regarding external forcing, we also tested the sea surface temperature (SST) anomalies associated with the stationary wave patterns and showed that the SST anomaly pattern forcing the teleconnections has changed. However, recent modeling studies indicate that pre-industrial droughts were driven by internal variability, with SST playing a secondary role (Coats et al., 2015; Stevenson et al., 2015).

To the knowledge of this author, only a few studies have investigated the linkage of drought event in the pre-industrial and paleoclimate era associated with the Dipole pattern. Cook et al. (2014) analyzed the last millennium drought and mentioned that the temperature and the 500hPa geopotential height anomalies pattern in the 1933-1934 winter is similar to the persistent circulation anomaly that dominated North American climate during the winter of 2013–2014. Therefore, it would be of special interest to examine the variability of the winter stationary wave in the pre-instrumental era.

Previous studies have mentioned that some teleconnection patterns may link to the 2013/14 drought, i.e., tropical Northern Hemisphere (TNH) (Marinaro et al., 2015), and Blob index (Bond et al. 2015). We include a number of teleconnection indices in this study examinate the Dipole variation's association with the various forcing sources. Meanwhile, a large and growing body of literature has investigated the interaction between the Arctic and mid-latitudes weather, linking the Arctic amplification (AA) to the changed circulation

over North America, despite some inconsistency. For example, Overland and Wang (2015) suggested that the Arctic influence will reinforce the regional geopotential height pattern and impact subarctic severe weather. Screen and Simmonds (2010) used the Fourier decomposition method to examines the large-scale changes over North Hemisphere. They point out that changes in meridional amplitude over recent decades are relatively small compared to the year-to-year variability. Also, they argue that the AA only affects the near surface temperature, and is weaker at 500 hPa. Although these studies show such a discrepancy of interpreting the AA impact and the response circulation, it implies the importance of the Arctic dynamics to North America. In this study, we also apply the AO index to represent the impact of the Arctic for the preliminary investigation.

## 3.2 Data and Methods

### 3.2.1 Additional Reanalysis Data

We applied additional datasets from Chaper 2, including (1) The Community Earth System Model (CESM) Large-Ensemble Project with 40 members (Kay et al. 2015) from 1950 to 2005 for the historical period and from 2040 to 2080 for the projected perspectives driven by Representative Concentration Pathways (RCP) 8.5 scenario; (2) the 21,000 year-long Paleoclimate simulation from 21,000 years before present into the pre-industrial era with the model ECBilt-CLIO which forced with the time-dependent ice-sheet topography, orbital forcing, and greenhouse gas forcing. In the model simulation, it includes the prognostic vorticity equation and the thermodynamic equation with a set of physical parameterizations of diabatic processes and coupled with an ocean model. The simulation started from a 2000 year-long Last Glacial Maximum equilibrium simulation. In this way, we could be able to validate the observed Dipole variation across all the datasets in the extended analysis period back to 21,000 B.P and into 2090 A.D. This global atmospheric model is based on a quasi-geostrophic adiabatic core with T21 resolution (64 points for longitude and 32 points for latitude) and three vertical layers: 200mb, 500mb, 800mb. Geopotential height data only available on 500mb with wintertime (DJF) mean. First year corresponds

to year 21,000 B.P. (Before Present: 1950 A.D.); the last year is to be interpreted as year 1 B.P. but with pre-industrial greenhouse gases. Although the paleoclimate measurements are limited, the simulation based on the atmospheric physics process can provide a decent dataset of the past.

### 3.2.2 Dipole and Climate Index

In Chapter 2, we refer the first mode of post-1980 EOF as the Dipole and use the corresponding PC as the index. Here, Dipole index was constructed by subtracting the $\triangle Z_E 250$ values between the ridge and trough centers from the $5^\circ \times 5^\circ$ averaged centered at (53°W,54°N) and (103°W,63°N), respectively. Wang et. al. (2014) used this Dipole index to illustrate the record event in the 2013–2014 winter. The mid-latitude weather and climate are induced by the trough-ridge system through the upper-level baroclinic process. Thus, the Dipole index which computed from 250 hPa geopotential height is adopted to reflect the standing circulation pattern. Note that the Dipole index in the paleoclimate data set was different from the reanalysis because of the discrepancy of the vertical level. In order to make it comparable, we used the least squares regression, where the dipole index from the 20CR reanalysis dataset is the independent variable, the dipole index from the paleoclimate data set is the dependent variable, with the time period is from 1981 to 1950 which is the overlapping period amount two data set.

Additional climate indices were used and these are provided by the Climate Prediction Center's climate monitoring website. In this study, we included various teleconnection indices includning: Western Pacific pattern (WP), Northern Oscillation index (NOI); Atmosphere index: Arctic Oscillation (AO), Northern Hemisphere pattern (TNH); ENSO index: Nino 4; Sea Surface Temperature index: Blob Index, Western North Pacific (WNP); Surface Temperature index: North American Winter Temperature Dipole (NAWTD), which Singh et al. (2016) used East-West coast surface temperature difference as an index.

### 3.2.3 Statistical Analysis

Dipole index was compared to the aforementioned climate indices for the years 1950-2016 using reanalysis datasets and 1851-2013 for retrospective re-analysis datasets. The 30-year running window variance and correlations were separately computed for Dipole index and each climate variable. The one-tailed approximate t-test was applied as well as Pearson's correlation coefficients were calculated to estimate statistical significance.

## 3.3 Results

### 3.3.1 Dipole Variance

The transition between the leading and secondary modes of atmospheric circulation during the 1980s, as we show in Chapter 2, suggests that the Dipole variance has increased (Singh et. al, 2016; Wang et al. 2015). To put the Dipole variances into historical and projected perspectives, we examined the CESM Large-Ensemble Project with 40 members and ECBilt-CLIO model for the paleoclimate simulation. By calculating the 30-year running variance of the Dipole index, we found that the Dipole variance has undergone a pronounced low-frequency fluctuation. As shown in Fig. 3.1 (a), an inter-decadal variation on the order of 60 years is observed, evidenced in the longer-term re-analysis data. Both the NCEP-NCAR and ERA-Interim re-analysis indicate that the Dipole variance was largest in the early $21^{st}$ century. We further tested PNA 30-year running variance with both NCEP-NCAR re-analysis I and 20CR datasets. To gain more insight into the relationship between the PNA and Dipole, we focus on the PNA/Dipole variance's contribution by comparing their respective percentages from the total variance. Fig. 3.1 (b) shows the anti-correlation between PNA and Dipole, a result that leads support to the sliding EOF analysis in Fig. 2.1 about the lead mode change.

A similar analysis of the CESM ensemble means to reveal the flucuation in Dipole variance during the historical period (up to 2005 with increasing greenhouse gas) shows that the Dipole variance is projected to continue increasing under the high-emission (RCP 8.5) scenario (Fig 3.1 a). However, the projected ensemble-mean variance starts to decline

after 2050, despite an increase in the ensemble spread; this suggests a rather uncertain future concerning the Dipole fluctuation. At this point, we can only attribute this late-21$^{st}$ century decline to the low-frequency natural variability as observed.

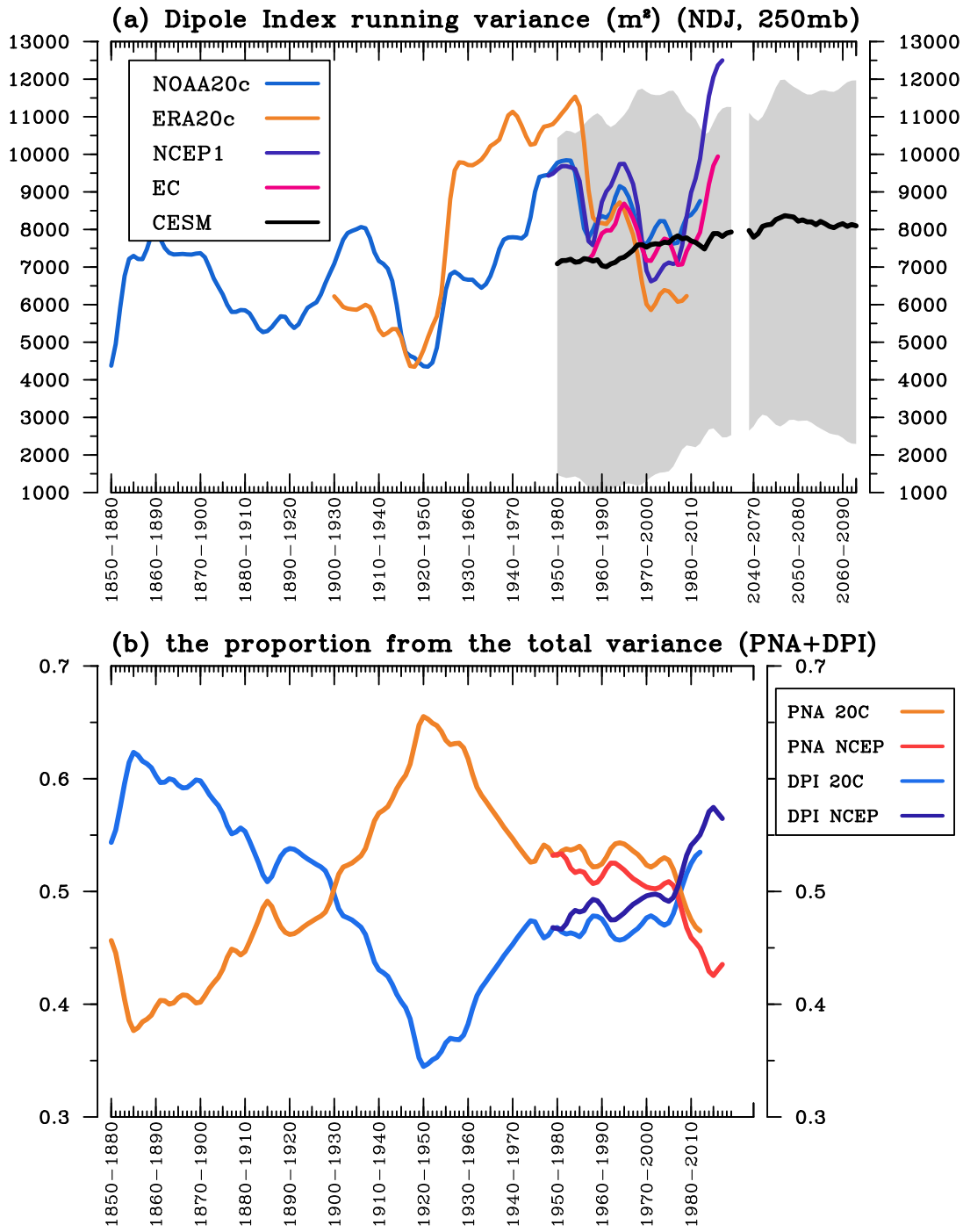


Fig. 3.1: (a) The 30-years running variance of the Dipole index derived from Wang et al. (2014) using multiple reanalysis data sets as indicated at upper left. Gray shaded represents the spread of CESM 40-member ensemble calculated from two standard deviations above and below the ensemble mean. (b) The 30-years running variance ratio of the PNA and the Dipole index, which were computed from NCEP-NCAR I and 20CR re-analysis data.

We use the same approach to compute the Dipole index from the paleoclimate data, albeit with a coarse spatial resolution. In addition, considering the much longer paleoclimate time scale, the running variance analysis has a 100-year period with 10-year intervals. The result of the Dipole index time series from the paleoclimate model data is one order larger than the Dipole index from the 20CR DJF mean. Different from the re-analysis data, the paleoclimate simulation is not a product of data assimilation, which may lead to such a discrepancy. However, the time series from both datasets has a similar fluctuation during the overlapping year from 1851 to 1950. In order to make the analysis comparable, least-squares regression method was applied. Figure 3.2 illustrates the reconstructive paleoclimate Dipole index series (blue line) and the global surface temperature mean (green line) superimposed with the 20CR wintertime Dipole 100-year running variance (red dot).

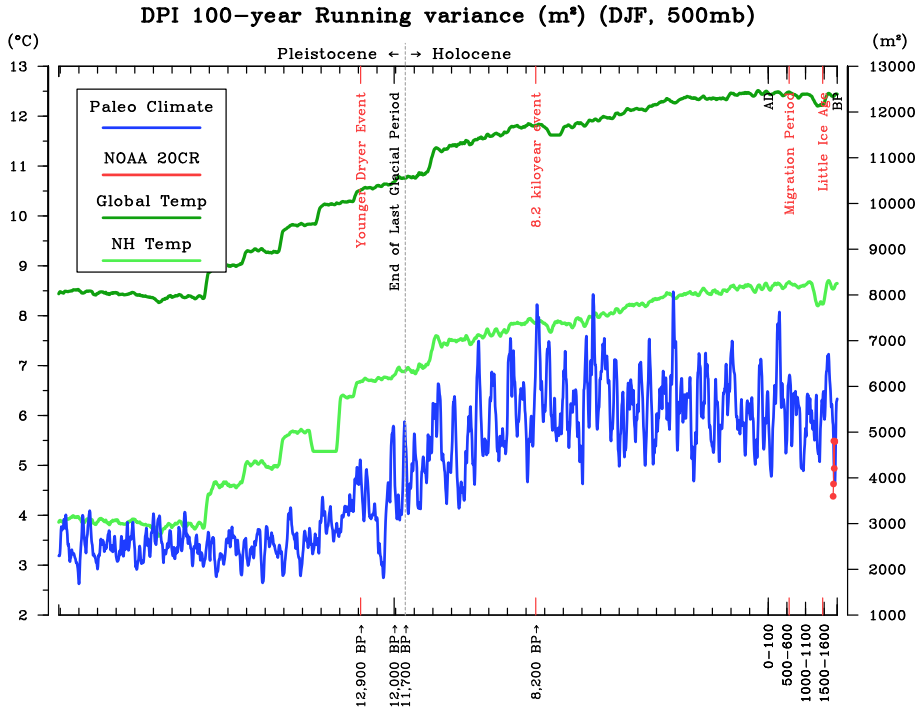


Fig. 3.2: The 100-years running variance of the Dipole index (DJF mean, 500 hPa) derived using paleoclimate and 20CR dataset as indicated at upper left. Green line represents the global temperature mean and light green for North Hemisphere temperature mean, and the historical events were noted.

Throughout the paleoclimate, we can see that the Younger Dryer event appears to be a "turning period". Before the Younger Dryer event, the global temperature is cooler and the Dipole index variance is relatively low and stable. After the Younger Dryer event, the global temperature decreased and lasted for about 1,200 years. The well-known hypothesis of the Younger Dryer event is that the thermohaline circulation changes, causing global cooling. Therefore, it can be inferred that SST and the thermal wind dynamics may be an important factor of the Dipole variance. In the era of Holocene, when the climate warmed again, the Dipole variance gradually increased until the average value which is about 5500 $m^2$, with a greater fluctuation. The 8.2 kiloyear event was a sudden decrease in global temperatures, which also related to the changes in the thermohaline circulation. The temperature changes were milder than the Younger Dryer event but was more severe than the Little Ice Age. Accrodingly, Dipole variance is likely associated with the global temperature: During the Pleistocene era, the global temperature is lower and the Dipole variance is smaller and less fluctuated; Since the Holocene with the increasing global temperature, the Dipole variance grew and became more fluctuated.

### 3.3.2 Forcing to Dipole

We next considered a number of climate indices which were shown to link with the signficant 2013/14 and 2014/15 events. Western Pacific pattern (WP), which represents a primary mode of low-frequency variability over the North Pacific, describes the anticyclonic anomaly over the Gulf of Alaska-Bering Sea and a cyclonic anomaly downstream over North America (Yu and Zhang, 2015); Western North Pacific (WNP) is defined as a specific SSTA pattern, forms one year before a full-fledged El Nino/La Nina, which has a growing connection between the WNP pattern and the development of ENSO in the following year since 1960 (Pegion and Selman 2017); and Niño 4, an index for the ENSO event since Dipole index was suggested to correspond with Niño 4 index in the following year (denoted as Nino4 (Y+1)) (Wang et al., 2014); Blob index, an anomalous high-pressure system induces clockwise surface wind anomalies that work against the prevailing surface westerlies to reduce local surface evaporation and weaken cold ocean advection in

the Northeast Pacific, giving rise to the Pacific warm blob during the 2014/15 California drought event (Bond et al. 2015); Northern Oscillation index (NOI) provides a superior covariate of interannual precipitation variability in Northern California (Mariza, 2016); tropical Northern Hemisphere pattern (TNH), which affects central U.S. winter temperature and storm track, affected the interior by cold-air outbreaks and the persistent western U.S. high-pressure that helped to establish extreme drought over California (Marinaro et al., 2015).

Arctic influence was also considered in 2013-2014, the Arctic Oscillation (AO) reached a strong positive phase, which allows further southward penetration of Arctic cold air masses and increases storminess into the mid-latitudes. For the surface temperature indicator, Singh et al. (2016) define North American Winter Temperature Dipole (hereby NAWTD), which directed from the difference of surface temperature of west and east coasts. Those indices were found to be connected with the 2013-2014 event, represting many processes that involve air-sea interaction and internal variability.

Recall in Figure 2.4 that the circulation pattern associated with the leading mode of winter circulation variations has significantly changed. Therefore, exploring the relationship between Dipole index and teleconnection indices can help us understand the relationship within those patterns. Here, all the aforementioned Climate indices were used to calculate the 30-year running correlation with Dipole index. The analysis included the NCEP re-analysis I (solid and dot lines) and 20CR dataset (long dash lines) datasets.

Figure 3.3 shows that only the Blob, Niño 4 (Y+1) and WNP indices have exceeded the significant level (0.46) in their 30-year running correlation analysis, which implies that the Dipole is linked to local SST anomalies in the Northeast and Northwest Pacific. This result is consistent with the previous study, suggesting that an ENSO precursor can form the Dipole through a teleconnection emanating from the WNP (Wang et. al, 2014). As mentioned in the last section, the Pacific warm Blob is induced by an anomalous high-pressure, allowing the excess solar radiation to warm up the surface sea temperature throughout the stable condition. This high-pressure could be linked to the abnormal ridge of the Dipole

pattern. Therefore, when the Dipole pattern developed, it would accompany the warmer SST underneath. Figure 3.3 shows that increasing high correlation between the Blob index and the Dipole index formed in the mid-20th century since 1960. The correlation between PNA and Dipole index is consisteatly low (0.2) during most of the analysis period, given their quater phase shift. In the post-1980 period, the Dipole correlation with the PNA index shows a steeply decreasing trend, while the correlations with NAWTD, TNH, Niño 4 (Y+1) indices shown an increasing trend after the mid-1970s, especially the AO. It infers that those indices combined could be a compounding mechanism that forms the Dipole pattern; this echoes the observation by Lee et al. (2014) that multiple factors from the tropics to high latitudes contributed to the abnormal amplification of the 2013/14 winter circulations. Preliminary results presented here suggested that investigating in air-sea interaction would be instrumental in understanding the dynamics of Dipole fluctuation.

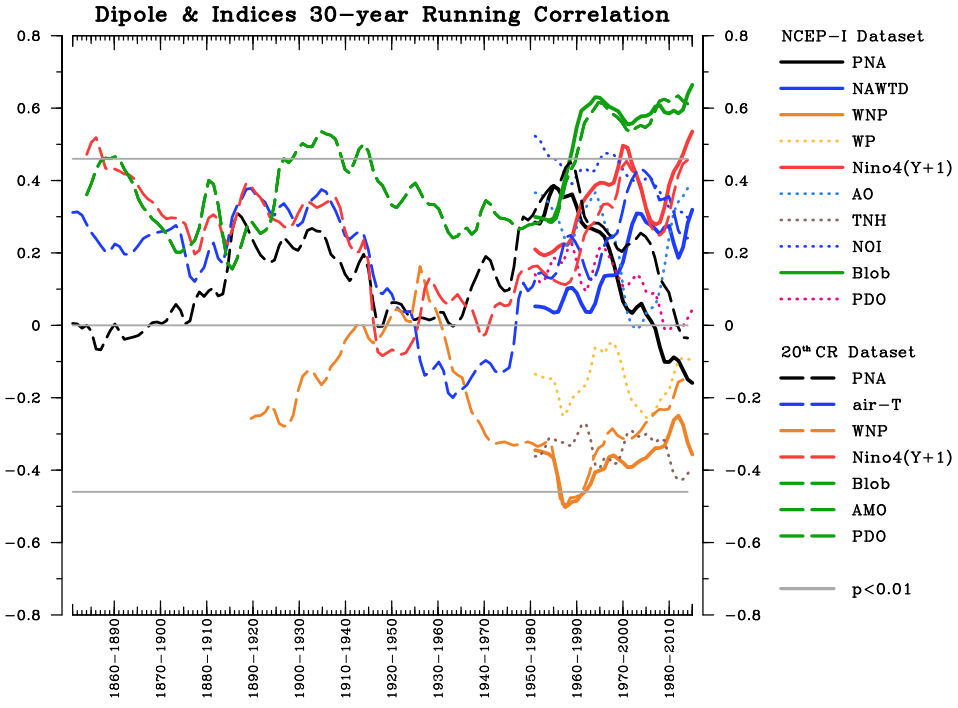


Fig. 3.3: 30-year running correlation of Dipole index and Climate indices. The solid lines and dots lines for NCEP reanalysis I dataset; the long dash lines for 20 CR dataset. Gray lines indicate significant value. ($p<0.01$)

### 3.4 Conclusion

This study focuses on long-term climate variability and the corresponding factors. We tested the Dipole variability by using multiple re-analysis and modeling datasets for the pre-industrial period and future projection. We found that the Dipole variance has undergone a pronounced low-frequency fluctuation. The Dipole variance in the paleoclimate suggests that the variance is related to the global temperature variation. Historical events such as the Younger Dryers event and the 8.2 kiloyear event, with substantial global temperature decreases, coexist with robust changes in the Dipole variance. The Dipole variance is relatively stable in the Holocene, which is a warmer era. In this study, the paleoclimate data we used is a low-resolution (64*32 grids) dataset. The Dipole index we calculated might come from a smoothed error and therefore cannot precisely depict the pattern. Although the low-resolution data does not represent the climate at the time, sufficient long-term climate data can give us a general idea of climate change and help us to have a preliminary understanding of paleoclimate. However, this part of the study only uses one paleoclimate dataset, without any comparison with other paleoclimatic simulations. Moreover, this model lacks feedback processes in the carbon cycle, vegetation, and terrestrial ice sheets. Ice sheet cover in our current pattern is different from the past, so the jet-terrain interaction might have impacted the circulation as well. These aspects require more complete simulations to reveal, which is outside the scope of this thesis.

We also tested the possible forcing by correlating the Dipole index with multiple large-scale climate indices that were associated with the record Dipole intensity in 2013/14 winter. The correlation results show that most of the indices are randomly correlated to the Dipole index, rarely exceeding the significant level. However, the indices related to the ocean response such as WNP and Niño 4 (Y+1) have reached the significant level, implying that the warming of the SST in the tropical West Pacific may provoke the changing stationary waves. Compared with the pre-1980 era, the downstream trough of the Dipole has intensified (Fig. 2.2), which can produce cold conditions in eastern North America. Overall, this study examines the pre-industrial climate variability and the forcing sources and its

result reveals that the tropical-extratropical, ocean-atmosphere, and Arctic-mid-latitude interactions associated to the Dipole pattern, combined with the internal low-frequency variation, can collectively alter the leading modes of North America's winter circulation variability.

# CHAPTER 4

# GENERAL CONCLUSIONS

Severe winter weather events in recent decades have become more frequent in North America, including extreme drought conditions in the Western regions and abnormally cold snaps in the Eastern continent. Those events can lead to resource management issues, such as water shortage, natural gas demand, transportation problem under hazardous weather, and even an impact on the ecosystem. The 2013-2014 California drought was particularly serious and has gained a lot of attention. Numerous studies (*e.g.*, Swain et al. 2014; Singh et. al. 2016; Wang et al. 2017; Swain et al. 2018) have investigated the circulation anomalies and the possible forcing during the events, but most of those studies did not link the abnormality to the stationary wave maintenance dynamics. In this study, we examined the perspective of the observed and projected changes of the wintertime stationary-wave circulations in North America.

In chapter 2, we compared the dominant circulation pattern during the pre- and post-1980 by the sliding EOF analysis. The diagnostics undertaken here suggest that the leading mode of Northern Hemispheric atmospheric stationary waves underwent a notable change. Since the 1980s, the first EOF mode of winter stationary eddies has changed from the PNA to the Dipole. Given that the EOF describes the variance of individual patterns, this finding also echoes the increased amplitude of the Dipole as observed. It implies that the marked increase in severe winter weather events associated with the Dipole pattern will increase, becoming a predominant mode than the PNA-associated precipitation and temperature anomalies, especially in the sub-seasonal timescale.

In chapter 3, we investigated the Dipole index variance in the distant past and projected future. The CESM large-ensemble simulations forced with increasing greenhouse gas indicate that the Dipole variance will generally amplify alongside its low-frequency natural variability. This result implies that the variation of the atmospheric circulations over North America,

especially in the sub-seasonal timescale, could continue to be dominated by the Dipole with the potential to sharpen the east-west division of temperature anomalies across North America. The results from paleoclimate simulation suggest that the temperature and the ocean currents may be the important internal forcing to the Dipole pattern. During the paleoclimate era, the global temperature and the ocean current experienced a pronounced change in the timescale of every thousand years based on the Younger Dryers event and the 8.2 kiloyear event. These events infer that the Dipole variance may be driven by the air-sea interaction, with a low-frequency variation component.

Overall, the presented analysis allows us to explore the long-term atmospheric feature associated with the recent change in extreme winter events. This research points out that the leading mode of wintertime circulation variability has undergone a low-frequency evolution from the PNA to the Dipole pattern. The change from the PNA to the Dipole is most pronounced in the sub-seasonal timescale, rather than in the seasonal timescale. Future studies should focus on the mechanism and the dynamic processes of sub-seasonal variation in the wintertime stationary waves, including the Jet-terrain interactions, tropical-extratropical interactions in terms of sub-seasonal variability. We note that the climate pattern during the paleoclimate merits detailed study, including to verify the dataset with different paleoclimate simulation and discuss the terrain effect in the different era.

# REFERENCES


[1] Bond, N. A., M. F. Cronin, H. Freeland, and N. Mantua, 2015: Causes and impacts of the 2014 warm anomaly in the NE Pacific. Geophys. Res. Lett., 42, 3414–3420, doi:10.1002/2015GL063306

[2] Chang, E. K. M., 2009: Diabatic and orographic forcing of northern winter stationary waves and storm tracks. J Climate, 22, 670–688. doi:10.1175/2008JCLI2403.1

[3] Francis, J. A., and S. J. Vavrus, 2012: Evidence linking Arctic amplification to extreme weather in mid-latitudes. Geophys. Res. Lett., 39, L068601, doi:10.1029/2012GL051000.

[4] Ganetis, S., and B. A. Colle, 2015: The thermodynamic and microphysical evolution of an intense snowbound during the northeast U.S. blizzard of 8–9 February 2013. Mon. Wea. Rev., 143, 4104–4125, doi: https://doi.org/10.1175/MWR-D-14-00407.1.

[5] Greybush, S. J., S. Saslo, and R. Grumm, 2017: Assessing the ensemble predictability of precipitation forecasts for the January 2016 and 2016 East Coast winter storms. Wea. Forecasting, 32, 1057–1078, https://doi.org/10.1175/WAF-D-16-0153.1

[6] Hartmann, D. L., 2015: Pacific sea surface temperature and the winter of 2014. Geophys. Res. Lett., 42, 1894–1902, doi:10.1002/2015GL063083.

[7] Huang, B., V.F. Banzon, E. Freeman, J. Lawrimore, W. Liu, T.C. Peterson, T.M. Smith, P.W. Thorne, S.D. Woodruff, and H.-M. Zhang, 2014: Extended Reconstructed Sea Surface Temperature version 4 (ERSST.v4): Part I. Upgrades and intercomparisons. Journal of Climate, 28, 911-930, doi:10.1175/JCLI-D-14-00006.1

[8] Higgins, R. W., J.-K. E. Schemm, W. Shi, and A. Leetmaa, 2000: Extreme precipitation events in the western United States related to tropical forcing. J. Climate, 13, 793–820, doi: 10.1175/1520-0442(2000)013¡0793:EPEITW¿2.0.CO;2.

[9] I. T. Jolliffe, Principal Component Analysis (Springer-Verlag, New York, 1989).

[10] Johnson, N. C., and S. B. Feldstein, 2010: The continuum of North Pacific sea level pressure patterns: Intraseasonal, interannual, and interdecadal variability. J. Climate, 23, 851–867. doi:10.1175/ 2009JCLI3099.1

[11] Kalnay, E., and Coauthors, 1996: The NCEP/NCAR 40-year reanalysis project. Bull. Amer. Meteor. Soc., 77, 437–472, doi: 10.1175/1520-0477(1996)077¡0437:TNYRP¿2.0.CO;2.

[12] Kay, J. E., and Coauthors, 2015: The Community Earth System Model (CESM) large ensemble project. Bull. Am. Meteorol. Soc., 96, 1333–1349, doi:10.1175/BAMS-D-13-00255.1.

[13] Kirtman, B. P., D. A. Paolino, J. L. Kinter III, and D. M. Straus,2001: Impact of tropical subseasonal SST variability on seasonal mean climate simulations, Mon. Weather Rev., 129, 853–868.

[14] Lee, M.-Y., Hong, C.-C. and Hsu, H.-H, 2015: Compounding effects of warm sea surface temperature and reduced sea ice on the extreme circulation over the extratropical North Pacific and North America during the 2013–2014 boreal winter. Geophys. Res. Lett. 42, 1612–1618.

[15] NOAA National Centers for Environmental Information (NCEI), 2019: U.S. billion-dollar weather and climate disasters. https://www.ncdc.noaa.gov/billions/.

[16] Overland, J.E. and Wang, M. (2015) Increased variability in early winter subarctic North American atmospheric circulation. Journal of Climate, 28, 7297–7305.

[17] Overland, J.E., and Coauthors, 2016: Nonlinear response of mid-latitude weather to the changing Arctic. Nature Climate Change, 6, 992–999, doi:10.1038/NCLIMATE3121.

[18] Pegion, K. V., and C. Selman, 2017: Extratropical Precursors of the El Niño–Southern Oscillation. Climate Extremes: Patterns and Mechanisms, 299-314.

[19] Schulte, J. A., and S. Lee, 2017: Strengthening North Pacific influences on United States temperature variability. Sci. Rep., 7, 124, doi:10.1038/s41598-017-00175-y.

[20] Screen, J. A., Simmonds, I. (2013). Exploring links between Arctic amplification and mid-latitude weather. Geophysical Research Letters, 40, 959–964. https://doi.org/10.1002/grl.50174

[21] Singh, D., and Co-authors, 2016: Recent amplification of the North American winter temperature dipole. J. Geophys. Res.: Atmos., 121, 9911-9928, doi:10.1002/2016JD025116.

[22] Swain, D. L., and Co-authors, 2014: The extraordinary California drought of 2013/2014: Character, context, and the role of climate change [in "Explaining Extremes of 2013 from a Climate Perspective"]. Bull. Amer. Meteor. Soc., 95, S3-S7.

[23] —, B. Langenbrunner, J. D. Neelin, and A. Hall, 2018: Increasing precipitation volatility in twenty-first-century California. Nature Climate Change, 8, 427.

[24] Takaya, K. and Nakamura. H, 2001: A formulation of a phase-independent wave-activity flux for stationary and migratory quasi-geostrophic eddies on a zonally varying basic flow. Journal of the Atmospheric Sciences 58(6), 608–627.

[25] Timm, O. and Timmermann, A, 2007: Simulation of the Last 21000 Years Using Accelerated Transient Boundary Conditions, J. Climate, 20, 4377–4401.

[26] Voelker, S. L., S.-Y. Wang, T. E. Dawson, J. S. Roden, C. J. Still, F. J. Longstaffe, and A. Ayalon, 2019: Tree-ring isotopes adjacent to Lake Superior reveal cold winter anomalies for the Great Lakes region of North America. Scientific Reports, 9: 4412, doi:10.1038/s41598-019-40907-w.

[27] Wang, S.-Y., L. Hipps, R. R. Gillies, and J.-H. Yoon, 2014: Probable causes of the abnormal ridge accompanying the 2013–2014 California drought: ENSO precursor and anthropogenic warming footprint. Geophys. Res. Lett., 41, 3220–3226. doi:10.1002/2014GL059748.

[28] —, W.-R. Huang, and J.-H. Yoon, 2015: The North American winter 'dipole' and extremes activity: A CMIP5 assessment. Atmos, Sci. Lett., 16, 338-345.

[29] —, J.-H. Yoon, E. Becker, and R. Gillies, 2017: California from drought to deluge. Nat. Climate Change, 7, 465-468.

[30] Zhang, X., A. Sorteberg, J. Zhang, R. Gerdes, and J. C. Comiso, 2008: Recent radical shifts of the atmospheric circulations and rapid changes in the Arctic climate system. Geophys. Res. Lett., 35, L22701, doi:10.1029/2008GL035607.

[31] Zhou Z.-Q., S.-P. Xie, X.-T. Zheng, Q. Liu, and H. Wang, 2014: Global warming-induced changes in El Niño teleconnections over the North Pacific and North America. J Climate, 27, 9050–9064, doi:10.1175/JCLI-D-14-00254.1.

[32] Greybush SJ, Saslo S, Grumm R, Greybush SJ, Saslo S, Grumm R. 2017. Assessing the ensemble predictability of precipitation forecasts for the January 2015 and 2016 east coast winter storms. Weather and Forecasting 32: 1057–1078, https://doi.org/10.1175/WAF-D-16-0153.1.